ISSN 1392–1320 MATERIALS SCIENCE (MEDŽIAGOTYRA). Vol. 18, No. 4. 2012

Electrodeposition and Photoelectrocatalytic Activity of ZnO Films on AISI 304 Type Steel

Agnė ŠULČIŪTĖ, Eugenijus VALATKA *

Department of Physical Chemistry, Kaunas University of Technology, Radvilenu pl. 19, LT-50254 Kaunas, Lithuania

crossref http://dx.doi.org/10.5755/j01.ms.18.4.3089

Received 12 July 2011; accepted 29 December 2011

Zinc oxide films on AISI 304 stainless steel were prepared by electrochemical deposition using slightly acidic zinc acetate solutions under galvanostatic conditions. The prepared films were characterized by X-ray diffraction, Fourier – transform infrared spectroscopy, scanning electron microscopy and photovoltammetry analysis. It was established that as-deposited ZnO films consist of lamellar particles with intercalated CH_3COO^- ions. It was determined that ZnO films show n-type behavior, the incident photon-to-current efficiency (IPCE) being 2.0 % at +0.6 V in 0.1 M K_2SO_4 solution. The observed steady-state photocurrents increased upon heat treatment at 673 K of as-deposited ZnO samples and in the presence of methanol in supporting electrolyte.
Keywords: zinc oxide, electrodeposition, oxide electrodes.

1. INTRODUCTION

Zinc oxide (ZnO) is an important semiconducting material in various industrial applications, such as catalysts, rubber and concrete additive, photovoltaics, pigments, gas sensors, mixed-oxide varistors [1]. ZnO crystallizes predominantly in the hexagonal wurtzite-type structure. It has been shown in numerous papers that ZnO films can be deposited using chemical vapour deposition, radio frequency magnetron sputtering, molecular beam epitaxy, sol-gel, hydrothermal synthesis, electrochemical deposition. Electrochemical deposition presents several advantages when compared to other methods [2, 3]: low cost, possibility of large-scale deposition, low temperature processing and direct control of film thickness. Very thin layers with specific composition, morphology and good adhesion between the deposited film and the substrate of complex shape can be prepared using the electrochemical techniques. The final morphology and texture of the electrodeposited material depend on the electrolyte composition, temperature, electrode potential or current density, duration of electrodeposition process and nature of the electrode substrate. Recently, the importance of several electrochemical methods in the synthesis of various semiconductor nanostructures was reviewed by Wu et al. [4]. Peulon and Lincot were first to demonstrate that the direct electrodeposition of ZnO films of good quality from aqueous solutions is possible [5]. This work generated a lively interest and intensive research followed in this field [6–27]. Conventional baths for the electrodeposition of zinc oxide typically contain $ZnCl_2$ or $Zn(NO_3)_2$. There is a leak information concerning ZnO electrodeposition using zinc acetate precursor. The presence of various organic molecules in the electrodeposition bath is known to highly influence the structure and properties of semiconductor films.

The aim of this work was to determine structure ad photoellectrocatalytic activity of electrodeposited ZnO films on stainless steel. This work is relevant to the development of functional materials and methods suitable for photoelectrocatalytic oxidation of organic compounds.

2. EXPERIMENTAL METHODS

2.1. Synthesis of zinc oxide

Zinc oxide films on stainless steel were prepared by electrochemical deposition under galvanostatic conditions. AISI 304 stainless steel plates 0.5 mm thick were used as a support. All solutions were prepared using doubly distilled water and analytical grade reagents. Zinc acetate ($Zn(CH_3COO)_2{\cdot}2H_2O$; >97 % purity) and potassium nitrate (KNO_3, purity >99 %) were obtained from Reachim (Russia) and used as received. Only freshly prepared solutions were used for the synthesis. All solutions were not deaerated during the experimental runs. The electrochemical deposition was carried out at 291 K – 343 K. The as-deposited samples were thoroughly washed with distilled water and dried to constant weight at room temperature. The as prepared samples were thermally treated under air atmosphere at 673 K for 1 h. The electrodeposition was carried out under galvanostatic conditions using 0.05 M $Zn(CH_3COO)_2$ + + 0.1 M KNO_3 + 0.001 M HNO_3 electrolyte (initial pH 5.8). In order to form ZnO films on steel substrate the current density was varied in the range of (0.10 – 1.5) mA cm^{-2}.

2.2. Analytical techniques

The electrochemical measurements were performed by computer-controlled Autolab PGSTAT12 (Ecochemie, The Netherlands) potentiostat/galvanostat, using a standard three electrode cell (volume 100 mL). The GPES® 4.9 software was used for the collection and treatment of the experimental data. The anodic compartment contained the

*Corresponding author. Tel.: +370-37-300153; fax.: +370-37-300152.
E-mail address: *evalatka@ktu.lt* (E. Valatka)

stainless steel working electrode and Ag, AgCl | KCl(sat) reference electrode. Throughout the paper all potentials are referred to this electrode. The cathodic compartment housed a platinum wire (geometric area about 15 cm^2) as a counter electrode.

The X-ray powder diffraction (XRD) data were collected with DRON-6 (Bourevestnik Inc., Russia) powder diffractometer with Bragg-Brentano geometry using Ni-filtered CuK_α radiation and graphite monochromator. The crystallite size D_{hkl} was calculated from the line broadening using the Scherrer's equation [28]:

$$D_{hkl} = \frac{k \cdot \lambda}{B_{hkl} \cdot \cos\Theta}, \quad (1)$$

where λ is the wavelength of the CuK_α radiation (1.54056×10^{-10} m), θ the Bragg diffraction angle, B_{hkl} the full width at the half maximum intensity of the characteristic reflection peak ($2\theta = 31.66°$, 34.38°, 36.26°) and k a constant (the value used in this study was 0.94).

Scanning electron microscopy (SEM) images were acquired using the Hitachi S-4800 scanning electron microscope operating at 2 kV accelerating voltage. Samples were imaged without any conductive coating.

FTIR spectra were measured in the range of 400 cm^{-1} – 4000 cm^{-1} on a Perkin Elmer FT-IR System infrared spectrometer using KBr pellets (1 mg of the substance was mixed with 200 mg KBr and these pellets was pressed in vacuum atmosphere).

The photoactivity of ZnO thin films was investigated using photovoltammetric method. A two compartment photoelectrochemical quartz cell was employed. The electrolyte volume in each compartment was the same (100 mL). The anodic compartment contained the ZnO working electrode and Ag, AgCl | KCl(sat) reference electrode. The cathodic compartment housed a platinum wire as a counter electrode. 0.1 M K_2SO_4 (purity >99%, Reachim, Russia) solution was used as a supporting electrolyte. The back side of the working electrode was insulated with the epoxy resin in order to eliminate its contribution to the dark current. The coated area of electrode was carefully positioned in the path of the UV irradiation. A General Electric F8W/BLB lamp was placed at a distance of 2 cm from the ZnO electrode and was used as an UV radiation source. The lamp emits mainly in the 315 nm–400 nm range, the peak wavelength λ_{max} being at 366 nm. The average power density at 366 nm was determined to be 1.8 mW cm^{-2} [29]. The incident photon-to-current efficiency (IPCE) value of a photoelectrode was calculated by using the following expression [30]:

$$\mathrm{IPCE}(\%) = 100\frac{1240 \cdot i_{ph}}{\lambda P}, \quad (2)$$

where i_{ph} is the photocurrent density in mA cm^{-2}, λ the wavelength of the incident light in nanometers (the value used in this study was 366 nm), P the incident light intensity in mW cm^{-2}.

The photoelectrocatalytic activity of the prepared films was also tested by using methanol as a model organic compound (CH_3OH, purity >99.5 %, Lachema, Czech Republic).

3. RESULTS AND DISCUSSION

3.1. Voltammetric behavior of stainless steel in zinc(II) acetate electrolyte

The voltammetric behavior of AISI 304 type stainless steel electrode in 0.05 M $Zn(CH_3COO)_2$, 0.1 M KNO_3 and 0.001 M HNO_3 electrolyte is shown in Fig. 1. Sweeping negatively from an initial potential of –0.28 V, a reductive peak (labeled C_1) is observed. The increase in cathodic current was observed at negative potential of –0.65 V. This peak can be related to the reduction of nitrate ions and formation of hydroxide ions [31]:

$$NO_3^- + H_2O + 2e^- \rightarrow NO_2^- + 2OH^-; \quad (3)$$

A further increase in observed currents at negative potential of –0.98 V can be mainly associated with water decomposition releasing molecular hydrogen and hydroxide ions:

$$2H_2O + 2e^- \rightarrow H_2 + 2OH^-; \quad (4)$$

As a result of these processes, the pH of the electrolyte close to the electrode increases. Hydroxide ions formed via electrochemical reduction are expected to react with Zn(II) ions present in electrolyte. Thus, zinc oxide is deposited on the electrodes according to the reaction (3):

$$Zn^{2+} + 2OH^- \rightarrow Zn(OH)_2 \rightarrow ZnO + H_2O; \quad (5)$$

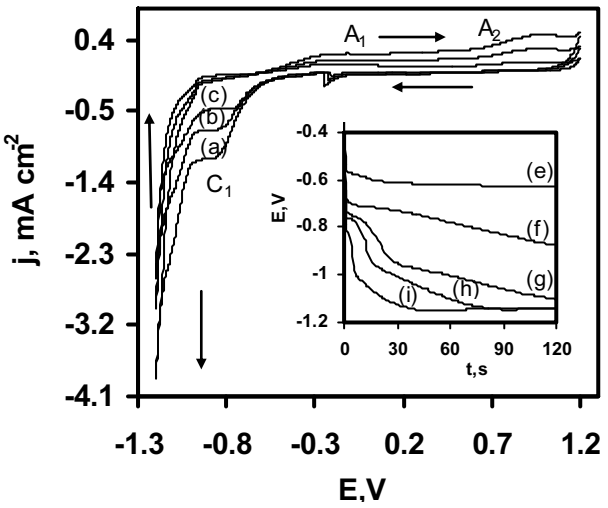

Fig. 1. Voltammetric behavior of AISI 304 type steel in 0.05 M $Zn(CH_3COO)_2$ + 0.1 M KNO_3 + 0.001 M HNO_3 electrolyte at 293 K and various potential scan rates (mV·s^{-2}): 50 (a), 25 (b), 10 (c). Inset: chronopotentiograms at different current densities (mA cm^{-2}): 0.10 (e), 0.25 (f), 0.50 (g), 0.75 (h), 1 (i)

In addition, some amount of OH^- ions can be supplied through hydrolysis as follows [32]:

$$CH_3COO^- + H_2O \rightarrow CH_3COOH + OH^- \quad (6)$$

This is very general scheme of cathodic electrodeposition of ZnO films using nitrate solutions. Other processes, such as the deposition of metallic zinc can take place and play an important role in the nucleation and the growth of nonstoichiometric ZnO_x films [11, 22, 25].

It can be assumed that zinc oxide electrodeposition in nitrate bath follows an EC (electrochemical reaction followed by an irreversible chemical reaction) mechanism. As it is pointed out in [31] the relative importance of (1) and (2) reactions in electrogeneration of base is not well-

established. Some experimental evidences show that hydrogen evolution reactions is as important as nitrate reduction in the electrodeposition of (hydro)oxides [31].

When the potential was reversed at –1.2 V and scanned towards the positive values, an increase of anodic current was observed at the potentials above –0.6 V. It was observed that the peak A_1 increases with an increase of electrolyte temperature and can be mainly associated with the oxidation of unidentified electrodeposited compounds. The increase of anodic current at the potentials above 0.8 V (A_2 peak) can be related to the evolution of oxygen and the oxidation of the stainless steel substrate. It has been shown [33] that the transpassive dissolution of stainless steel occurs due to the release of soluble Cr(VI) and Fe(III) species into the electrolyte.

In order to form zinc oxide coatings, a galvanostatic method was used. The current density of electrodeposition was varied in the range of $(0.10-1.5)\ \mathrm{mA\,cm^{-2}}$ and electrolysis duration 2 min – 30 min. The characteristic chronopotentiograms are shown in the inset of Fig. 1. The preliminary electrolysis experiments revealed that the most stable coatings are obtained at $1\ \mathrm{mA\,cm^{-2}}$. At higher current densities the rapid thickening and flaking of the deposits was observed. Thus, during following experiments we used the zinc oxide electrode prepared under the experimentally determined optimal conditions: cathodic current density $1\ \mathrm{mA\,cm^{-2}}$, electrolysis duration 10 min, electrolyte temperature 333 K – 343 K.

3.2. Structural characterization of zinc oxide films

XRD analysis of as-deposited at 343 K samples showed three peaks at $2\theta = 31.66$, 34.38 and 36.26°, thus suggesting a crystalline ZnO structure (Fig. 2). The strong low-angle reflection peak at $2\theta \approx 7°$ can be associated with acetate groups intercalated into zinc oxide structure.

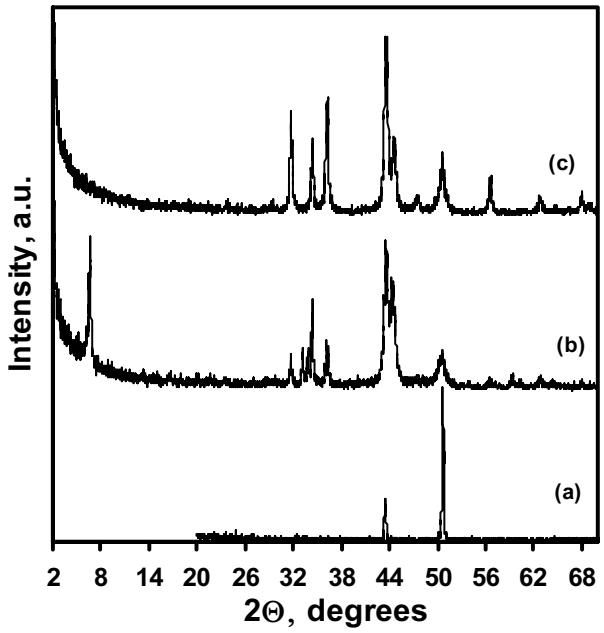

Fig. 2. XRD pattern of stainless steel (a), as-deposited (b) and annealed at 673 K (c) ZnO electrode

The formation of layered basic zinc acetate could not be excluded, however, a more detailed structure characterization of as-deposited films is needed in order to confirm this assumption. XPS analysis of the prepared films is currently under investigation and the results will be published in a separate paper.

After the heat-treatment at 673 K for 1 h, the XRD analysis reveals diffraction peaks corresponding to the well-crystallized ZnO. According to the Scherrer's equation, the average ZnO crystallite size was calculated to be 29 nm.

SEM images of as-deposited and annealed zinc oxide films are shown in Fig. 3. The as-deposited (Fig. 3, a) ZnO film is lamellar. It is seen that the annealing at 673 K for 1 h considerably change the surface to granular (Fig. 3, b). The diameter of grains are between 30 nm and 110 nm.

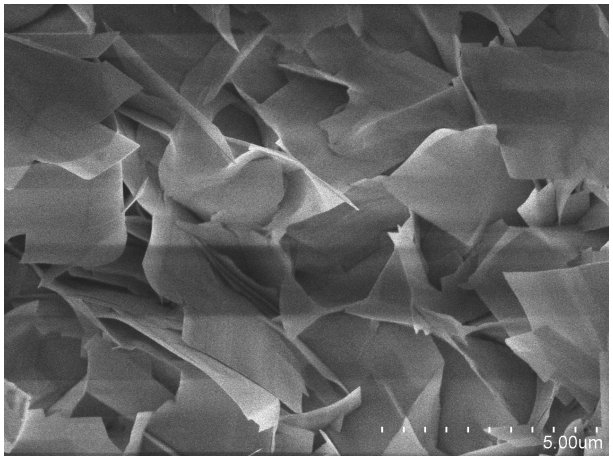

a

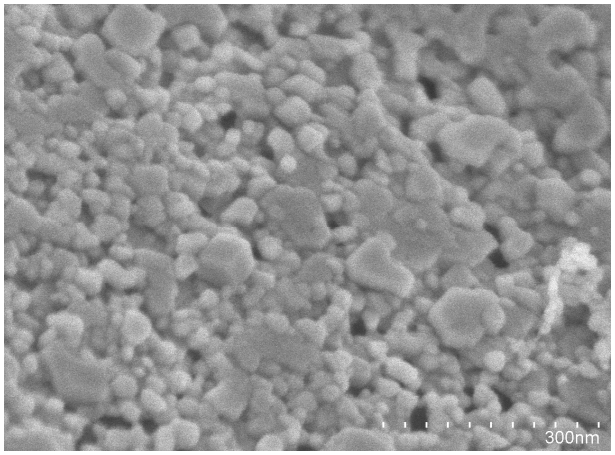

b

Fig. 3. Representative SEM images of as-deposited (a) and annealed at 673 K (b) ZnO films

The incorporation of acetate ions in as-prepared zinc oxide films is confirmed by infrared absorption analysis too (Fig. 4). It presents the IR absorption not only in the low ($600\ \mathrm{cm^{-1}} - 400\ \mathrm{cm^{-1}}$) wave number region as it would be expected for pure ZnO [32], but in the intermediate ($1600\ \mathrm{cm^{-1}} - 800\ \mathrm{cm^{-1}}$) and high ($3300\ \mathrm{cm^{-1}} - 3700\ \mathrm{cm^{-1}}$) wave number region as well, due to vibrations of impurities ions. The large absorption band centered at $3476\ \mathrm{cm^{-1}}$ can be assigned to the stretches of hydroxy groups.

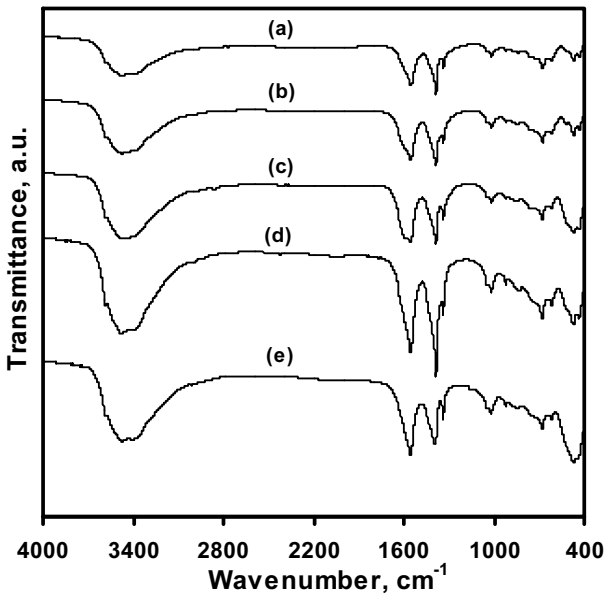

Fig. 4. FTIR spectra of as-deposited zinc oxide obtained at various temperatures (K): 303 (a), 313 (b), 323 (c), 333 (d), 343 (e)

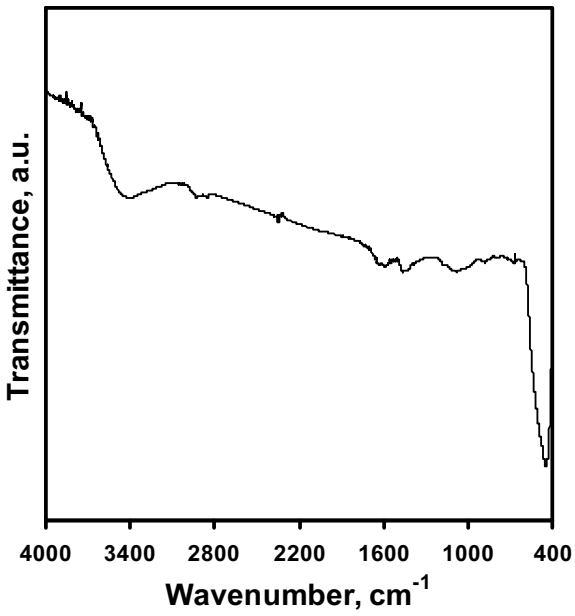

Fig. 5. FTIR pattern of zinc oxide annealed at 673 K

The peaks observed at 1555 cm^{-1} and 1396 cm^{-1} can be attributed to the asymmetrical and symmetrical stretching vibrations of the acetate ions, respectively. Other peaks at 1338, 1019 and 677 cm^{-1} shows the presence of CH_3 groups [34]. A broad band centered at 472 cm^{-1} corresponds to the characteristic stretching frequency of Zn–O bond and it can be used for the identification of zinc white pigment in the IR spectra of real paint sample layers [35]. The obtained experimental results show that this characteristic band becomes more intense with the increase of synthesis temperature.

3.3. Photoelectrocatalytic properties of ZnO films

The photoelectrochemical behavior of ZnO electrode was determined from the current-potential curves obtained in 0.1 M K_2SO_4 solutions both in the dark and under UV irradiation (Fig. 6).The potential was swept from –0.3 V to +1.0 V at 10 mV s^{-1}. The behavior of electrode is characteristic of the n-type semiconductor [37]. The observed anodic photocurrent can be related to the generation of hydroxyl radicals ($^{\bullet}OH$) and other oxidation products (e. g., H_2O_2) at the surface of ZnO electrodes [38]. The hydrogen peroxide is known to be formed as a result of the interaction of hydroxyl radicals [29].

For n-type semiconductor, the photocurrent is due to the diffusion or the migration of charge carriers, depending on whether semiconductor film is particulate or continuous, respectively. In a case of thick and continuous film, a depletion layer can be developed upon contact with electrolyte facilitating the separation of photogenerated holes and electrons. According to Gartner-Butler model [39], the presence of the depletion layer can be determined by plotting the square of the photocurrent density, i_{ph}^2, with respect to the applied potential, E. Fig. 6 inset shows that the plots i_{ph}^2 vs E are linear in the rising parts of the photovoltammograms, thus, confirming the formation of the depletion layer in the prepared films.

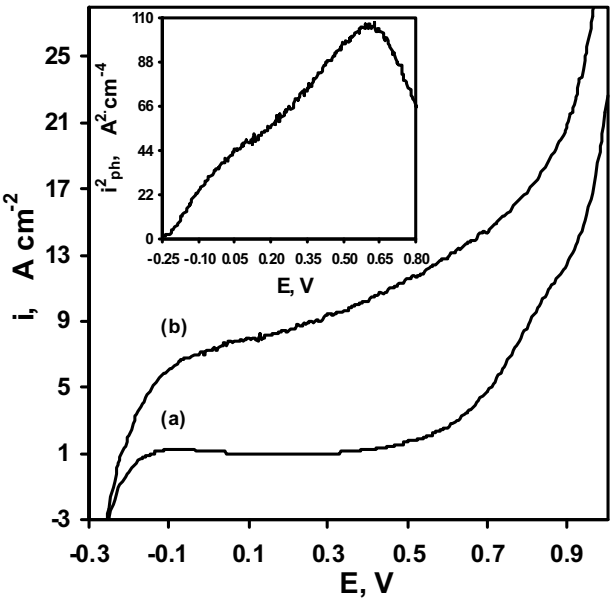

Fig. 6. Characteristic voltammograms in the dark (a) and under UV illumination (b) of ZnO electrode deposited at 333 K. Potential scan rate v = 10 mV s^{-1}, 0.1 M K_2SO_4 solution at 291 K. Inset: Plot of the square of the photocurrent density, i_{ph}^2, with respect to the applied potential, E

Based on the photocurrent measurements, the incident photon-to-current efficiency (IPCE) values of ZnO photoelectrode were calculated and shown in Fig. 7. It was found that these values are comparable to those for Degussa P25 TiO_2 electrode measured under identical experimental conditions [29].

The time dependence of the electrode current in the dark and under UV irradiation for the ZnO electrode is presented in Fig. 8. In a case of as-deposited ZnO sample when the light was switched on, the observed current jumped to about +0.04 A and reached a steady-state value.

When the light was switched off, the current of the ZnO decreased and reached its initial value. The presented

results show that the photocurrents are increased upon heat-treatment at 673 K.

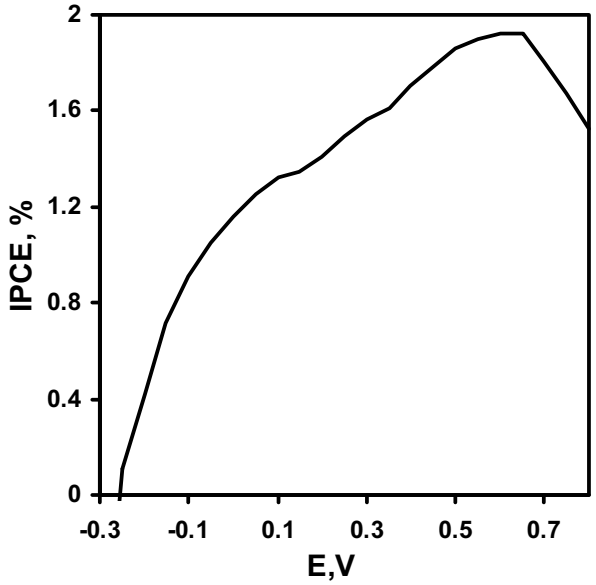

Fig. 7. The incident photon-to-current efficiency (IPCE) values for ZnO in 0.1 M K_2SO_4 electrolyte

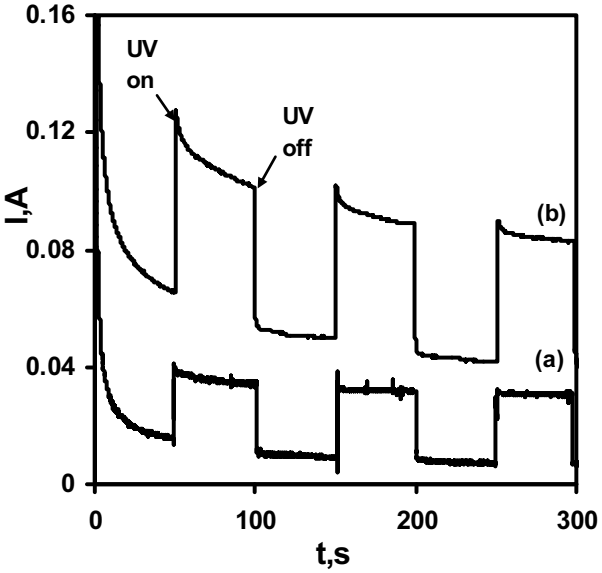

Fig. 8. Chronoamperometry curves in 0.1 M K_2SO_4 solution in the dark and under UV illumination of ZnO electrode deposited at 343 K (a) and ZnO electrode deposited at 343 K and annealed at 673 K for 1 hour (b)

The results in Fig. 9 show that the steady state photocurrent increases with the increase in methanol concentration.

It has been stated [40] that the increase in observed photocurrent with substrate concentration suggests that the interaction of these compounds and their partially-degraded intermediates with the oxide surface does not inhibit the photohole capture process. In order to establish the mechanism of photoelectrochemical oxidation of water dissolved pollutants, a kinetic model was developed [41]. It has been demonstrated that methanol oxidation mainly proceeds through an indirect hole transfer mechanism, via surface bound hydroxyl radicals, followed by the so-called current-doubling effect [42].

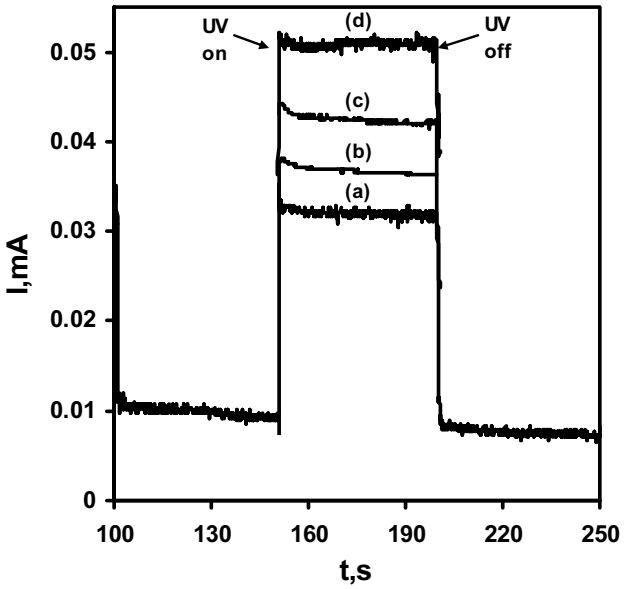

Fig. 9. Chronoamperometry curves of ZnO electrode deposited at 343 K in the dark and under UV illumination in 0.1 M K_2SO_4 solution and different methanol concentration (M): 0 (a), 0.001 (b), 0.002 (c), 0.003 (d)

It is generally assumed [38, 42] that methanol molecules interact weakly with the oxide surface, they are not specifically adsorbed and do not compete with water molecules to be adsorbed on oxide surface. On the contrary, strong and specific adsorption seems to be a necessary condition for the direct hole mechanism, as is a case for formic acid [42].

CONCLUSIONS

Zinc oxide films on AISI 304 type stainless steel were prepared using the electrochemical deposition from slightly acidic zinc(II) acetate solution under galvanostatic conditions. Electrochemical measurements revealed that zinc oxide deposition occurs at negative potential of –0.9 V. It was established that the most uniform and stable films were obtained at 1 mA cm^{-2}, electrolysis duration being 10 min. XRD, SEM and FTIR analysis confirmed that the as-deposited ZnO is composed of lamellar particles with intercalated acetate ions. Such structure is destroyed during annealing at 673 K with the formation of particulate ZnO films an average crystallite size being 29 nm. The obtained n-type ZnO films are highly photoactive and the observed photocurrents in K_2SO_4 electrolyte increase upon addition of methanol.

REFERENCES

1. **Klingshirn, C.** ZnO: Material, Physics and Applications *A Europian Journal of Chemical Physics and Physical Chemistry* 8 2007: pp. 782 – 803.
2. **Corni, I., Ryan, M. P., Boccaccini, A. R.** Electrophoretic Deposition: from Traditional Ceramics to Nanotechnology *Article Journal of the European Ceramic Society* 28 2008: pp. 1353 – 1367.
3. **Boccaccini, A. R.; Zhitomirsky, I.** Application Of Electrophoretic And Electrolytic Deposition Techniques In Ceramics Processing *Current Opinion in Solid State & Materials Science* 6 2002: pp. 251 – 260. http://dx.doi.org/10.1016/S1359-0286(02)00080-3

4. **Wu, X.-J., Zhu, F., Mu, C., Liang, Y., Xu, L., Chen, Q., Chen, R., Xu, D.** Electrochemical Synthesis And Applications Of Oriented And Hierarchically Quasi-1D Semiconducting Nanostructures *Coordination Chemistry Reviews* 254 2010: pp. 1135 – 1150. http://dx.doi.org/10.1016/j.ccr.2010.02.014

5. **Peulon, S., Lincot, D.** Cathodic Electrodeposition From Aqueous Solution Of Dense Or Open-Structured Zinc Oxide Films *Advanced Materials* 8 1996: pp. 166 – 169. http://dx.doi.org/10.1002/adma.19960080216

6. **Peulon, S., Lincot, D.** Mechanic Study of Cathodic of Electrodeposition of Zinc Oxide and Zinc Hydroxychloride Films from Oxygenated Aqueous Zinc Chloride Solutions *The Journal of The Electrochemical Society* 145 1998: pp. 864 – 874.

7. **Gu, Z. H., Fahidy, T. Z.** Electrochemical Deposition of ZnO Thin Films on Tin-Coated Glasses *The Journal of The Electrochemical Society* 146 1999: pp. 156 – 159. http://dx.doi.org/10.1149/1.1391579

8. **Pauporté, T., Lincot, D.** Electrodeposition of Semiconductors for Optoelectronic Devices: Results on Zinc Oxide *Electrochimica Acta* 45 2000: pp. 3345 – 3353.

9. **Pauporté, T., Lincot, D.** Hydrogen Peroxide Oxygen Precursor for Zinc Oxide Electrodeposition II – Mechanistic Aspects *Journal of Electroanalytical Chemistry* 517 2001: pp. 54 – 62. http://dx.doi.org/10.1016/S0022-0728(01)00674-X

10. **Yoshida, T., Komatsu, D., Shimokawa, N., Minoura, H.** Mechanism of Cathodic Electrodeposition of Zinc Oxide Thin Films from Aqueous Zinc Nitrate Baths *Thin Solid Films* 451 – 452 2004: pp. 166 – 169.

11. **Canava, B., Lincot, D.** Nucleation Effects on Structural and Optical Properties of Electrodeposited Zinc Oxide on Tin Oxide *Journal of Applied Electrochemistry* 30 2000: pp. 711 – 716.

12. **Katayama, J., Izaki, M.** Observation of Photocurrent Generation in Electrodeposited Zinc Oxide Layers *Journal of Applied Electrochemistry* 30 2000: pp. 855 – 858.

13. **Pauporte, T., Lincot, D.** Hydrogen Peroxide Oxygen Precursor for Zinc Oxide Electrodeposition I. Deposition in Perchlorate Medium *The Journal of The Electrochemical Society* 148 2001: pp. C310 – C314.

14. **Zhang, L. Chen, Z., Tang, Y., Jia, Z.** Low Temperature Cathodic Electrodeposition of Nanocrystalline Zinc Oxide Thin Films *Thin Solid Films* 492 2005: pp. 24 – 29.

15. **Goux, A., Pauporte, T., Chivot, J., Lincot, D.** Temperature Effects on ZnO Electrodeposition *Electrochimica Acta* 50 2005: pp. 2239 – 2248. http://dx.doi.org/10.1016/j.electacta.2004.10.007

16. **Fathy, N., Ichimura, M.** Electrochemical Deposition of ZnO Thin Films from Acidic Solutions *Journal of Crystal Growth* 294 2006: pp. 191 – 196.

17. **Xu, L., Guo, Y., Liao, Q., Zhang, J., Xu, D.** Morphological Control of ZnO Nanostructures by Electrodeposition *The Journal of Physical Chemistry* 109 2005: pp. 13519 – 13522.

18. **Lee, J., Nam, S. C., Tak, Y.** On the Origin of Electrodeposition Mechanism of Zno on ITO Substrate *Korean Journal of Chemical Engineering* 22 2005: pp. 161 – 164

19. **Gao, X.-D., Peng, F., Li, X.-M., Yu, W.-D., Qiu, J.-J.** Growth of Highly Oriented ZnO Films by the Two-step Electrodeposition Technique *Journal of Materials Science* 42 2007: pp. 9638 – 9644.

20. **Xu, L., Chen, Q., Xu, D.** Hierarchical ZnO Nanostructures Obtained by Electrodeposition *Journal of Physical Chemistry* 111 2007: pp. 11560 – 11565.

21. **Ramirez, D., Silva, D., Gomez, H., Riveros, G., Marotti, R. E., Dalchiele, E. A.** Electrodeposition of ZnO Thin Films by Using Molecular Oxygen and Hydrogen Peroxide as Oxygen Precursors: Structural and Optical Properties *Solar Energy Materials and Solar Cells* 91 2007: pp. 1458 – 1461. http://dx.doi.org/10.1016/j.solmat.2007.04.017

22. **Inamdar, A. I., Mujawar, S. H., Sadale, S. B., Sonavane, A. C., Shelar, M. B., Shinde, P. S., Patil, P. S.** Electrodeposited Zinc Oxide Thin Films: Nucleation and Growth Mechanism *Solar Energy Materials and Solar Cells* 91 2007: pp. 864 – 870. http://dx.doi.org/10.1016/j.solmat.2007.01.018

23. **Inamdar, A. I., Sonavane, A. C., Sharma, S. K., Im, H., Patil, P. S.** Nanocrystalline Zinc Oxide Thin Films by Novel Double Pulse Single Step Electrodeposition *Journal of Alloys and Compounds* 495 2010: pp. 76 – 81.

24. **Inamdar, A. I., Mujawar, S. H., Patil, P. S.** The Influences of Complexing Agents on Growth of Zinc Oxide Thin Films from Zinc Acetate Bath and Associated Kinetic Parameters *International Journal of Electrochemical Science* 29 2007: pp. 797 – 808.

25. **Palms, D., Norwig, J., Wegner, G.** Electrochemically Induced Growth of Zinc Oxide *A Europian Journal of Chemical Physics and Physical Chemistry* 8 2007: pp. 782 – 803.

26. **Lu, X.-H., Wang, D., Li, G.-R., Su, C.-Y., Kuang, D.-B., Tong, Y.-X.** Controllable Electrochemical Synthesis of Hierarchical ZnO Nanostructures on FTO Glass *The Journal of Physical Chemistry* 113 2009: pp. 13574 – 13582

27. **Altuntasoglu, O., Matsuda, Y., Ida, S., Matsumoto, Y.** Syntheses of Zinc Oxide and Zinc Hydroxide Single Nanosheets *Journal of Materials Chemistry* 22 2010: pp. 3158 – 3164.

28. Azaroff, L. V. Elements of X-ray Crystallography. Mc Graw Hill Book Co, New York, 1968.

29. **Valatka**, E., **Kulėšius**, Ž. TiO_2-mediated Photoelectrochemical Decoloration of Methylene Blue in the Presence of Peroxodisulfate *Journal of Applied Electrochemistry* 37 2006: pp. 415 – 420.

30. **Georgieva, J., Armyanov, S., Valova, E., Puolios, I., Sotiropoulos, S.** Enhanced Photocatalytic Activity of Electrosynthesised Tungsten Trioxide–Titanium Dioxide Bi-Layer Coatings under Ultraviolet and Visible Light Illumination *Electrochemistry Communications* 9 2007: pp. 365 – 370.

31. **Therese, G. H. A., Kamath, P. V.** Electrochemical Sythesis of Metal Oxides and Hydroxides *Chemistry of Materials* 12 (5) 2000: pp. 1195 – 1204.

32. **Huihu, W, Changsheng, X, Dawen, Z.** Controlled Growth of ZnO by Adding H_2O *Journal of Crystal Growth* 250 2007: pp. 372 – 377.

33. **Betova, I., Bojinov, M., Laitinen, T., Mäkelä, K, Pohjanne, P., Saario, T.** The Transpassive Dissolution Mechanism of Highly Alloyed Stainless Steels: I. Experimental Results and Modelling Procedure *Corrosion Science* 44 2002: pp. 2675 – 2697.

34. **Ishioka, T., Shibata, Y., Takahashi, M., Kanesaka, I., Kitagawa, Y., Nakamura, K. T.** Vibrational Spectra and Structures of Zinc Carboxylates I. Zinc Acetate Dihydrate *Spectrochimica Acta Part A* 54 1998: p. 1827. http://dx.doi.org/10.1016/S1386-1425(98)00063-8

35. **Vahur, S., Teearu, A, Leito, I.** ATR-FT-IR Spectroscopy in the Region of 550–230 $cm^{-1}$for Identification of Inorganic Pigments *Spectrochimica Acta Part A* 75 2010: pp. 1061 – 1072.

36. **Duan, Y., Li, J., Yang, X., Hu, L., Wang, Z., Liu, Y., Wang, C.** Kinetic Analysis on the Non-isothermal Dehydration by Integral Master-plots Method and TG–FTIR Study of Zinc Acetate Dihydrate *Journal of Analytical and Applied Pyrolysis* 83 2008: pp. 1 – 6.

37. **Rajeshwar, K.** Fundamentals of Semiconductor Electrochemistry and Photoelectrochemistry *I Encyclopedia of Electrochemistry* 6 2002: pp. 3 – 53.

38. **Turchi, C. S., Ollis, D. F.** Photocatalytic Degradation of Organic-Water Contaminants – Mechanisms Involving Hydroxyl Radical Attack *Journal of Catalysis* 122 (1) 1990: p. 178 – 192. http://dx.doi.org/10.1016/0021-9517(90)90269-P

39. **Georgieva, J., Armyanov, S., Valova, E.** Morphology, Structure and Photoelectrocatalytic Activity of TiO_2/WO_3 Coatings Obtained by Pulsed Electrodeposition onto Stainless Steel *Journal of Electroanalytical Chemistry* 585 2005: pp. 35 – 43. http://dx.doi.org/10.1016/j.jelechem.2005.07.018

40. **Houas, A., Lachheb, H., Ksibi, M.** Photocatalytic Degradation of Various Types of Dyes (Alizarin S, Crocein Orange G, Methyl Red, Congo Red, Methylene Blue) in Water by UV-irradiated Titania Applied *Catalysis B: Environmental* 31 2001: pp. 145 – 157. http://dx.doi.org/10.1016/S0926-3373(00)00276-9

41. **Lana Villarreal, T., Gomez, R., Neumann-Spallart, M.** Semiconductor Photooxidation of Pollutants Dissolved in Water: A Kinetic Model for Distinguishing between Direct and Indirect Interfacial Hole Transfer. I. Photoelectrochemical Experiments with Polycrystalline Anatase Electrodes under Current Doubling and Absence of Recombination *The Journal of Physical Chemistry B* 108 2004: p. 15172 – 15181.

42. **Hykaway, N., Sears, W. M., Morisaki, H., Morrison, S. R.** Current-doubling Reactions on Titanium Dioxide Photoanodes *The Journal of Physical Chemistry* 90 1986: pp. 6663 – 6667.